TraQuad: A Modular Tracked Legged Multi-modal Quadrupedal Robot

Alok Ranjan[§,†], *Student Member, IEEE*, Francesco Iotti§,[§,†], *Student Member, IEEE*, Franco Angelini[§,†], *Member, IEEE,*, Manolo Garabini[§,†], *Member, IEEE*

***Abstract*—The authors have developed a novel multi-modal robot named TraQuad, which integrates the features of legged and tracked robots. This robot aims to combine agility, maneuverability, traction, and efficiency for traversing various environments. Legged locomotion allows the robot to select optimal contact points on the terrain, while tracked locomotion enables faster movement over relatively simpler uneven terrains with greater efficiency. TraQuad can turn about its central vertical axis and execute sharp turns with a 0.25 m turn radius. It can climb steep slopes of 31° at a velocity of 0.9 m/s. Utilizing multi-modal locomotion, it can climb rocks and overcome obstacles by either skipping or stepping on them. Climbing rocks 1.75 times the height of the tracks requires a peak torque of 5.14 Nm, whereas stepping on a block of the same height requires a peak torque of 8.15 Nm. Skipping a block 1.5 times the height requires a peak torque of 11.8 Nm. This demonstrates that climbing obstacles while maintaining contact with them is more economical than stepping on them, proving the viability of tracked-legged locomotion. These advancements highlight the potential of TraQuad as a robust solution for navigating diverse and challenging environments.**

***Index Terms*—multi-modal locomotion, tracked, legged robots.**

I. Introduction

EXPLORING uneven terrains presents a significant challenge for robotic systems, requiring adaptive interactions with ground features to maintain stability [1], [2]. Advances in design and control continuously enhance their agility and efficiency in such environments [3]. Early autonomous robotic exploration predominantly relied on wheeled robots (WRs) due to their simple design, effective control, balanced weight distribution, load capacity, speed, and efficiency. These systems have evolved from fixed suspensions, such as Lunokhod [4], to more advanced designs like the rocker-bogie system employed in Spirit, Opportunity [5], and Curiosity [6]. The incorporation of differential suspension geometries further improved stability by ensuring even pressure distribution across wheels [7], [8].

This research is partially supported by the European Union's HORIZON-MSCA-2023-SE-01-01 - MSCA Staff Exchanges 2023 Program under the Grant Agreement No 101182891(NEUTRAWEED), Horizon 2020 Research and Innovation Programme under Grant Agreement No. 101016970 (Natural Intelligence), and Horizon Research and Innovation Programme under Grant Agreement No. 101070596 (euROBIN), and in part by the Italian Ministry of Education and Research in the framework of the "FoReLab" (Future-oriented Research Lab) Project (Departments of Excellence).

F. Iotti is within the Italian Doctorate in Robotics and Intelligent Machines.

[§]Centro di Ricerca "Enrico Piaggio", Università di Pisa, Largo Lucio Lazzarino 1, 56126 Pisa, Italy. [†]Dipartimento di Ingegneria dell'Informazione, Università di Pisa, Largo Lucio Lazzarino 1, 56126 Pisa, Italy.

Corresponding Author: Alok Ranjan alok.ranjan@phd.unipi.it

Fig. 1. The TraQuad robot prototype.

However, wheel sinkage in granular, muddy, or friable terrain often leads to traction loss, as observed in NASA's Opportunity rover [9]–[11]. Due to their relatively small contact patches, wheels may not always provide adequate traction [12]. While WRs navigate around obstacles by steering, climbing over obstacles can be particularly challenging. Despite these limitations, mobile robots continue to demonstrate significant potential in applications such as search and rescue, logistics, interplanetary exploration, and environmental monitoring.

In rough, uneven terrains, tracked robots (TRs) offer advantages over wheeled locomotion. For a given size and mass, tracks distribute shear stress over a greater contact length than wheels, reducing ground pressure and improving traction [12]. Additionally, deformable tracks conform to terrain features, enabling adaptability to hard, soft, yielding, and irregular surfaces. Their superior weight distribution minimizes sinkage in granular terrains, enhancing mobility across diverse substrates. Despite lower speed and efficiency compared to wheeled systems, their terrainability remains a key advantage [13]. Conventional TRs typically feature a box chassis with tracks spanning the full robot length. Examples include the Pan Tilt Trackbot, designed for surveillance and inspection, and Komodo-01, developed for agricultural applications [14]. However, these robots struggle with climbing obstacles exceeding their height due to constraints in surface friction and center of gravity (CG) positioning. To address this, Dyjob [15] integrates an adjustable CG mechanism to enhance step-climbing capabilities, though this adds weight and complicates payload placement. Alternative approaches employ body articulations to assist in pulling or crawling over obstacles. Body articulation can also be implemented by segmenting the robot, allowing one segment to function as articulation for the others. For instance, angle-changeable tracked robots [16], MACbot [17], and PackBot [18] incorporate front articulations. PackBot, a combat-proven, man-portable UGV, has been deployed in Afghanistan and Iraq for hazardous material detection. Similarly, the Aladdin crawler robot [19] features articulations on both the front and rear. More advanced designs, such as Karo [20] and the system proposed in [21], utilize four tracked arms, with rear segments capable of lifting the body during climbing, increasing the maximum surmountable height.

Legged robots (LRs) excel in traversing uneven terrains due to their ability to avoid obstacles and strategically select footholds, mimicking animal-like intelligent locomotion. This capability is crucial for navigating complex environments where precise terrain interaction is required. Unlike wheeled and TRs, which maintain continuous ground contact, LRs engage selectively with terrain features, enhancing maneuverability [22], [23]. However, they are generally slower, less energy-efficient, and more complex to control than their wheeled and tracked counterparts [24]. Notable quadrupedal LRs include Spot [1], ANYmal [25], Unitree Go[2], Mini Cheetah [26], HyQ [27], Oncilla [28], and Cheetah-cub [29], etc.

Each type of ground-based locomotion has distinct advantages and limitations. WRs excel in structured environments due to their speed and efficiency, while TRs and LRs perform better in unstructured terrains. TRs provide superior traction, whereas LRs navigate obstacles with greater adaptability. To leverage these strengths, hybrid robots integrating multiple locomotion strategies have been developed, offering innovative mobility solutions. Despite their complex design and control requirements, multi-modal robots enhance agility, maneuverability, and efficiency by combining different anatomical and control features.

For example, the WheTLHLoc robot [30] has two tracks for differential steering, two legs with actuated wheels, and two omni-wheels at the rear, providing three modes of locomotion. For instance, the WheTLHLoc robot [30] integrates two tracks for differential steering, two actuated legs with wheels, and two omni-wheels at the rear, enabling three locomotion modes: omni-wheels with normal wheels, purely tracked, or tracked-wheeled-legged mode, with the legs aiding in climbing obstacles. In recent years, wheeled-legged robots have gained prominence due to their versatility in structured and unstructured environments. Notable examples include the Swiss-Mile robot [31], Momaro [32], CENTAURO [33], BIT-NAZA [34], TAWL [35], and Hylos [36]. The Swiss-Mile robot, an extension of ANYmal with non-steerable, torque-controlled wheels, demonstrates dynamic motion capabilities in challenging environments, reducing transport costs by up to 85% compared to its purely legged counterpart [37]. Momaro employs four legs with steerable wheels, enabling omnidirectional movement and step climbing. CENTAURO, featuring four 5-degree-of-freedom (DOF) legs and two 7-DOF arms, provides enhanced dexterity and redundancy. Important wheeled biped robots include Handle[3], Ascento [38], BHR-WI [39], and Ollie [40]. However, hybrid locomotion remains relatively unexplored due to its complexity and the absence of direct biological analogs, making it challenging to establish fundamental principles for seamlessly integrating walking and driving. Addressing these challenges could enable hybrid robots to surpass natural locomotion systems in versatility and efficiency [31].

For exploration in uneven terrains, notable tracked-legged robots (TLRs) include CHIMP [41] and TITAN X [42]. CHIMP is a large, heavy robot with 39-DOF, a near-human form factor, and the strength and dexterity to operate in hazardous environments. Its track modules on both hands and legs enable locomotion on all four appendages or its knees [41]. TITAN X, resembling modern quadrupeds like ANYmal and Spot, features tracks proximal to the body and legged limbs distal. However, this configuration may not fully exploit the traction benefits of tracked systems.

We are interested in tracked-legged locomotion with tracks attached as end effectors due to the clear advantages of tracked systems in uneven terrains. Therefore, we propose a quadruped robot with tracked feet on the distal ends to achieve additional traction in all configurations. A comparison between the proposed design and a capable TR like PackBot highlights PackBot's strong suitability for most outdoor scenarios due to its terrainability and short adjustable tracks at the front, which facilitate obstacle negotiation and stair climbing. However, the PackBot design lacks the obstacle avoidance capability inherent to legged robots. In the proposed configuration, obstacle avoidance is achieved by lifting the base, allowing obstacles to pass underneath. Additionally, obstacles can be climbed, stepped on, or skipped, providing greater adaptability. In contrast, the PackBot design permits only climbing, without the ability to step directly on obstacles-a feature beneficial in scenarios requiring selective avoidance of ground patches, such as protected vegetation. Furthermore, the relatively smaller contact patch of the proposed design reduces terrain disruption, minimizing potential harm to micro-ecosystems.

This work contributes to the design and control scheme of a novel multi-modal tracked-legged robot, named TraQuad, as shown in Fig. 1. The robot features a modular design utilizing EM-Act actuators [43]. To assess the performance of the tracked system, a single-limb tracked actuator was first developed and tested. Subsequently, the full robot was designed, assembled, and tested in laboratory and natural settings. This paper presents the torque requirements on the hip and ankle joints of TraQuad to overcome various obstacles, including climbing steep slopes and rocks, as well as skipping or stepping on obstacles. Furthermore, the robot's steering capability is demonstrated. Additionally, a control system is developed to integrate the tracked and legged modalities. To facilitate multi-modal operation, an algorithm named StabiliTrack is deployed, illustrating how multi-modal traversal across different obstacles enhances movement capability compared to using a single modality.

II. TraQuad Design

In this section, the design and control scheme of the robot are discussed. TraQuad is an 8-DOF floating-base modular robot consisting of four legs, each with a tracked-foot end effector. The tracks enable faster movement over moderately uneven terrains, while the legs allow the foot to be lifted

[1]https://support.bostondynamics.com/s/article/Spot-Specifications-49916
[2]https://shop.unitree.com/
[3]https://bostondynamics.com/legacy/

to climb, skip, or step over obstacles. To better approach obstacles, the end effector orientation can be adjusted when the foot is lifted. First, the modular design of a single leg with a tracked foot is presented. This leg design is then replicated, and the design and control scheme of the full robot are outlined. Modularity is emphasized in the tracked-legged robot design to enhance dexterity. The focus is placed on a simpler configuration, which can be extended by incorporating additional actuation modules.

A. Mass and size of the robot

To introduce modularity in the robot design, an actuator named EM-Act [43] is considered. This actuator is designed in the shape of a limb, incorporating a motor, encoder, motor driver, and a compound gear-belt reduction gearbox. It can be connected as a chain link, enabling the robot to increase its DOF by linking additional actuators, allowing it to traverse complex environments. In the next subsection, the torque requirements for the tracks are calculated to assess the viability of the actuator in a tracked robot configuration.

It is observed that popular quadruped robots such as ANYmal-D (50 kg), Spot (33.8 kg), and Unitree Go 1 (12 kg) are relatively heavy. Inspired by the lighter Unitree Go1, to push the envelope, the aim is to limit the fully equipped tracked-legged robot to 10 kg. Using the EM-Act actuator that weighs 0.5 kg (revised version) helps achieve this goal. The weight of the robot chassis, including the battery and Raspberry Pi computers, is estimated at approximately 1.65 kg, allowing for a margin of 0.6 kg per actuator/limb and 0.3 kg per tracked foot in a 12-DOF configuration. This results in an estimated robot weight of approximately 7 kg for the 8-DOF configuration and 9 kg for the 12-DOF configuration.

The robot's size is defined by the actuator length. The body length equals the length of two actuators attached to its sides for hip actuation. The maximum height and length in extended configurations are determined by adding more actuators and end-effectors to the hip joint. These dimensions allow the robot to fold neatly, minimizing storage volume in a closed configuration. For the tracked foot, a configuration meeting the weight requirement of approximately 0.3 kg is aimed for, as lighter feet reduce energy consumption when lifting. Commercial metallic tracked chains are too heavy, exceeding 0.5 kg per foot. Alternatively, rubberized tracked tires offer lighter options. Three viable choices were identified: *1)* the *LEGO Technic Tracks* wheel kit, which is very lightweight but fragile and prone to belt elongation; *2)* the *XS-59606RD* tracked foot from *Xtra Speed*, weighing 0.325 kg; and *3)* the *Traxxas8880* tracked wheels from *Traxxas*, weighing 0.387 kg. The best option is selected by calculating the traction force produced by each track belt.

B. Torque and speed requirements for tracks

To move the tracks in uneven, sandy, and scree environments, a torque requirement of 5 to 10 Nm per tracked wheel is considered. The maximum speed requirement is set at 1 m/s on flat terrain and 0.5 m/s on slopes. The traction performance of the different tracked feet is assessed by calculating the traction

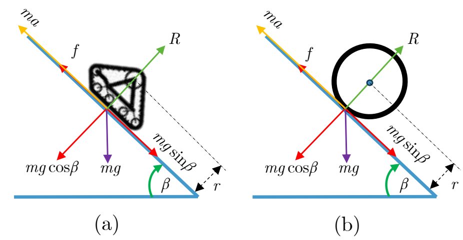

Fig. 2. Free body diagrams of a tracked foot (a) and an equivalent-sized wheel (b) climbing a slope (β).

force each foot generates and comparing it to an equivalent wheel, demonstrating the superiority of the tracked foot in terms of traction. It is assumed that the robot is climbing a 45° slope. The traction force is computed using the Mohr-Coulomb Failure criterion [12], where the shear force on the wheel-soil interaction surface is provided as:

$$F = cA + w \ \tan\phi \tag{1}$$

Here, c denotes the cohesion coefficient, A represents the contact patch area with the ground, w is the normal force acting on the contact patch due to the robot's weight, and ϕ signifies the angle of internal shearing resistance of the ground material. The values for c and ϕ, derived from experiments on a rough trench Asol135 [44], are 6.0 and 37°, respectively. These experiments were conducted for the Mars exploration rovers Spirit and Opportunity, and the same terrain data is used in the analysis. For the Lego belt tracked foot, with a contact patch of 80 mm $\times$ 20 mm and a weight of approximately 0.1 kg, the traction force is 61.35 N. The second tracked wheel, *XS-59606RD*, with a patch dimension of 150 mm $\times$ 45 mm, generates a traction force of 92.25 N. The third commercial tracked wheel, *TRX8880*, with a patch dimension of 174 mm $\times$ 51 mm, produces a traction force of 105 N. In comparison, a normal wheel with a contact patch of 10 mm $\times$ 45 mm generates a traction force of 54.45 N.

The *TRX8880* model is 19.08% heavier than the *XS-59606RD* but provides only 12.75 N (13.82%) more traction. Lego belt tracks exhibit slightly higher traction than wheels. Among the available options, the *XS-59606RD* tracks offer a superior trade-off between weight, traction, and robust design, capable of bearing the system load without visible deflection. These tracks provide approximately 70% more traction than wheels. To determine the most compatible tracked foot for the actuator, the torque requirements for both the *XS-59606RD* and *TRX8880* models were calculated. Assuming the traction force is aligned with the inclined ground, the force equilibrium, shown in Fig. 2, involves the ground reaction force (R) and frictional force (f). The maximum uphill climbing acceleration is set at 0.5 m/s^2. The torque arm (r) for the *XS-59606RD* and *TRX8880* models is 57 mm and 80 mm, respectively.

To ensure the robot's safety, if only one track is pulling the whole robot uphill, the torque required to climb the slope can be given as

$$\tau = fr = m(a + g\sin(\beta))r. \tag{2}$$

Here, $\beta = 45°$, $m = 7\,\text{kg}$ is the targeted mass of the robot, and g represents the gravitational acceleration. From equation (2), the required torque for the *XS-59606RD* is 2.97 Nm. For the *TRX8880*, the required torque is 4.16 Nm. Con-

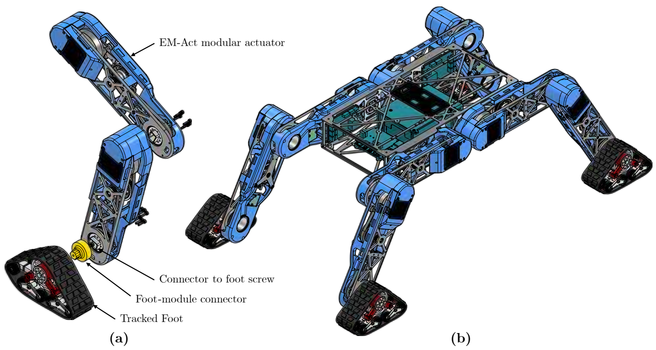

Fig. 3. (a) 3D model of the tracked foot with EM-Act modular actuators to create a leg configuration, (b) 3D model of TraQuad robot.

sidering 10% mechanical and electrical losses in transmission efficiency, these values adjust to 3.27 Nm and 4.58 Nm, respectively. Therefore, the *XS-59606RD* represents a more balanced choice in terms of traction force, compactness, and the torque that can be handled by the actuator.

Compiling all the data for the available options in Tab. I, it is observed that the wheeled foot exhibits the highest traction force per unit patch area (T/A) due to its minimal contact patch. However, T/A alone is insufficient as a selection criterion. A tracked foot enhances traction and mitigates slippage through cohesion force (*cA*), which scales with contact patch area. *LEGO Technic Tracks* provide a high traction ratio but have a limited torque capacity (3.8 Nm). *Traxxas8880* offers maximum traction but demands high nominal torque (4.16 Nm). For the EM-Act actuator, a nominal torque of approximately 2.5 Nm is required. Therefore, *XS-59606RD* is the optimal choice, balancing torque and traction range.

C. Tracked leg design

The EM-Act actuator [43] incorporates an Antigravity 5006 KV450 motor from T-Motor. With a 2-stage 9:1 reduction gearbox, it delivers a rated torque of 2.5 Nm and a peak torque of 19.6 Nm. Based on the mass and torque requirements outlined in Sec. II-A and II-B, the actuator meets the torque demands of *XS-59606RD*. Its modular design enables serial connections for multi-DOF configurations, allowing one actuator to manipulate another as a limb. Thus, the robot design is developed using these actuators.

To connect the tracked foot and modular actuator, a fastening part was designed. Extending this to a 2-DOF leg, an additional actuator was assembled on top, analogous to an animal's lower limb-where the lower actuator represents the thigh and the upper actuator represents the torso, connected at the hip joint. Introducing a knee joint would enhance reachable space, facilitate precise foot placement, distribute hip torque, and enable more walking gaits. A hip abduction/adduction joint would improve lateral balance, expand the support polygon, and enable 3D foot placement. A 16-DOF configuration would allow for more natural, animal-like gaits.

In the current configuration, the tracked foot joint functions as the ankle, enabling foot rotation and track actuation. When lifted, the foot rotates about its actuation axis. When the foot is in contact with the ground, the track belt revolves around the roller mechanism, changing its shape, incurring rolling resistance. When the foot is lifted, the energy required to rotate the tracked foot about its actuation axis is less than the rolling resistance of the track belt. Hence, the ankle joint rotates instead of moving the track belt. This helps orient the foot into the required configuration to achieve an optimal approach angle for foot-obstacle interaction. The CAD assembly of a single leg with tracks is shown in Fig. 3(a), with an exploded view detailing component connections.

TABLE I
END-EFFECTOR SELECTION CRITERIA

Foot type	**Traction Force (T)**	**Patch area (A) (mm^2)**	**(T/A)**	**r**	**T$_{min}$**	**T$_{max}$**
Wheeled foot	54.45	450	0.121	57	2.97	3.1
LEGO Technic Tracks	61.35	1600	0.038	62	3.23	3.8
XS-59606RD	92.25	6750	0.014	57	**2.97**	**5.25**
Traxxas8880	105	8874	0.012	80	4.16	8.4

D. Robot design

TraQuad is constructed by attaching four 2-DOF legs to a custom rectangular chassis that houses all essential electronics. The legs are symmetrically positioned along the sagittal plane. The complete robot design is depicted in Fig. 3(b), with specifications provided in Tab. II. The 8-DOF robot features hip flexion and track rotation capabilities. Future iterations could include knee rotation and hip abduction/adduction movements, enhancing foot placement and movement flexibility. This design emphasizes the tracked foot's capability to climb steep slopes, a challenge for legged and wheeled robots. The robot can also lift a leg to navigate obstacles, placing the foot back on the ground afterward. The robot is designed to showcase the integration of modularity and multi-modality. Demonstrating these capabilities is expected to enhance dexterity and performance in future iterations of TraQuad. Notably, the 8-DOF TraQuad is easier to control and performs efficiently on uneven terrain.

E. Robot Kinematics

To control the robot in any environment, an understanding of its kinematics is essential. The TraQuad consists of four legs, each equipped with two actuators. Adjusting the joint angle between these actuators modifies the robot's height. Each leg features a tracked foot as an end-effector, facilitating forward and backward movement as well as steering. The robot operates in two kinematic modes: one for controlling the tracked foot velocity and another for actuating hip rotation, with the potential for extension to additional joints if the DOF is increased.

1) Tracked System: The tracked platform kinematics follows a two-tracked vehicle model [45]. At any given time, the left tracked feet operate with a uniform linear velocity V_l, and the right tracked feet with a uniform linear velocity V_r. A difference between these velocities induces a steering action, generating an angular velocity ω_z at the robot base. This also results in translation velocities v_x and v_y along the X and Y axes, respectively, producing a velocity vector $\vec{V}$ for the robot base. The direct kinematics of the robot can be expressed as:

$$(v_x, v_y, \omega_z) = f_d(V_l, V_r). \tag{3}$$

To determine the control actions that achieve the desired motion, the inverse kinematics problem is presented as follows:

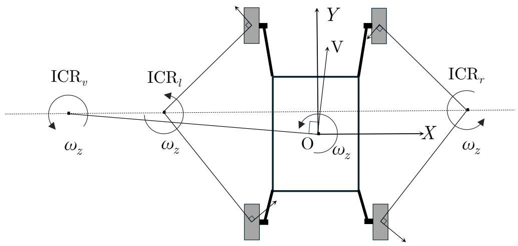

Fig. 4. General representation of the instantaneous centers of rotation for TraQuad's tracked system. When TraQuad is in a symmetric configuration, the line intersecting ICR_v, ICR_l, and ICR_r will also pass through the center of the base (O).

$$(V_l, V_r) = f_i(v_x, v_y, \omega_z). \tag{4}$$

If the robot is considered a rigid body with planar motion, as shown in Fig. 4, the instantaneous center of rotation (ICR_v) is defined as a point in the horizontal plane around which the motion of the robot base involves only rotation and no translation. In local coordinates, $ICR_v = (x_{ICRv}, y_{ICRv})$. In addition to considering the entire robot as a rigid body, both left tracks and both right tracks can also be treated as individual rigid bodies. In the local frame, the left tracks will have an instantaneous center of rotation $ICR_l = (x_{ICRl}, y_{ICRl})$. Similarly, the right tracks will have an instantaneous center of rotation $ICR_r = (x_{ICRr}, y_{ICRr})$. These left and right ICRs are defined on the ground plane, not around their roll axes. The local coordinates for the robot and track ICRs can be calculated geometrically as a function of the robot's translational and angular velocities.

$$x_{ICRv} = -v_y/\omega_z, \tag{5}$$

$$x_{ICRl} = (V_l - v_y)/\omega_z, \tag{6}$$

$$x_{ICRr} = (V_r - v_y)/\omega_z, \tag{7}$$

$$\text{and } y_{ICRv} = y_{ICRl} = y_{ICRr} = v_x/\omega_z. \tag{8}$$

The inverse functions can be computed from equations (5) - (8). The instantaneous translational and rotational speeds with respect to the local frame can then be expressed as:

$$v_x = \frac{V_r - V_l}{x_{ICRr} - x_{ICRl}} y_{ICRv}, \tag{9}$$

$$v_y = \frac{V_r + V_l}{2} - \frac{V_r - V_l}{x_{ICRr} - x_{ICRl}} \left(\frac{x_{ICRr} + x_{ICRl}}{2}\right), \tag{10}$$

$$\text{and } w_z = \frac{V_r - V_l}{x_{ICRr} - x_{ICRl}}. \tag{11}$$

The inverse kinematic relations can be expressed by

$$V_l = v_y + \omega_z x_{ICRl}, \tag{12}$$

$$V_r = v_y + \omega_z x_{ICRr}. \tag{13}$$

Here, x_{ICRl} and x_{ICRr} are estimated through steering experiments conducted over multiple trials on a flat surface. A wheeled differential drive is considered, with the wheels positioned on the ICRs. Only a particular configuration for which ICRs are identified is used during steering action.

2) Legged System: The legged system is designed to lift the foot to overcome obstacles. This allows obstacles to be avoided or the curvature of the obstacle to be followed, maintaining a favorable base orientation and ensuring adequate traction. Additionally, the robot's height can be adjusted, or it can be tilted to position the center of gravity favorably, enhancing stability while overcoming obstacles. From Fig. 5, in the two-dimensional plane S, the forward kinematic model for the shank link can be written as

$$O_f^s = \begin{cases} l\cos(q_i), & \text{along } X \text{ axis} \\ l\sin(q_i), & \text{along } Z \text{ axis} \end{cases} \tag{14}$$

Where l is the length and $q_i, i = [1, 2, 3, 4]$ are the joint angles of the thigh links.

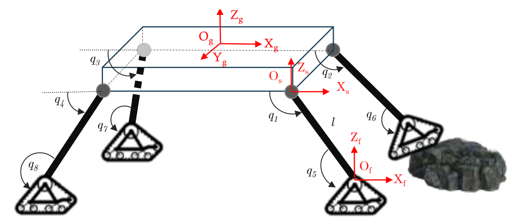

Fig. 5. Kinematic model of the TraQuad robot. Here, q_i represents the joint angle that is controlled by the respective actuator.

F. Control scheme of TraQuad

TraQuad consists of eight modular actuators that drive four hips and four tracked feet. Each actuator comprises a three-phase brushless Antigravity 5006 KV450 motor, driven by a Moteus r4.8 32-bit microcontroller (MC). The MC is integrated with a magnetic encoder, which detects motor position and calculates current consumption via a magnet on the motor shaft. Power is supplied to the motor driver from a DJI TB47D 4500 mAh battery through power distributors. Four power distributors are used, one for each leg, powering both motor drivers (hip, tracked foot) in parallel. The electronic control system includes a Raspberry Pi controller with a Pi3hat communication interface, which communicates directly with the motor driver. A Wi-Fi module in the Raspberry Pi controller allows communication of Python-coded control scripts from a PC to the robot and facilitates the acquisition of lower-level system data from sensors. Sensor data is read at a frequency of 500 Hz. Encoders, current, and temperature sensors (operating frequency: 15-30 kHz) are present on the motor driver, and an IMU sensor (operating frequency: 1 kHz) is integrated within Pi3hat. Data is transmitted serially to the motor drivers: the Raspberry Pi sends data to the first motor driver, which then relays it to the second motor driver. A PID controller in the motor driver ensures the correct functionality of the system [43].

In this 8-DOF version of TraQuad, a single control scheme manages both the tracked and legged systems simultaneously, enabling multi-modal locomotion. The control scheme is shown in Fig. 6. When no obstacles are present, actuation shifts to minimal use of actuators, relying solely on the tracked wheels. The robot's twist (i.e., v_x, v_y, and ω_z) is based on the tracked system kinematics from (12) and (13), from which V_l and V_r are obtained. A gain correlates the linear velocity of the tracked foot with the actuator's angular velocity. The low-level controller takes only the velocity reference as input. To handle obstacles that the tracked system alone cannot manage, a multi-modal locomotion strategy is employed, actuating both track and hip joints simultaneously. Actuating the hip helps the foot follow required trajectories, effectively managing obstacle avoidance. An algorithm named StabiliTrack, presented in Alg.1, integrates torque-based joint control and IMU-based joint control. Torque-based control relies on actuator torque data correlated with the actuator's current requirement (I), while IMU-based control utilizes IMU data from the Pi3hat. Both controls proportionally manage the hip joints (q_{hip}). A gait generator is also implemented to overcome obstacles that require the foot to be lifted. A vision system can provide the obstacle height and distance from the robot, which the robot can utilize to skip or step on it. This robot is not equipped with a vision system; therefore, obstacle information needs to be provided manually to lift the foot to skip or step on them. Low-level control for the hip takes position and velocity references as input.

1) StabiliTrack Algorithm: This algorithm outputs the desired hip (q_{hip}) angles to climb or descend any obstacle. It requires the torque on the tracked foot motors (τ_{track}), roll (θ_R), and pitch (θ_P) angles from the IMU sensor, and the forward velocity of the base (v_x) as inputs. Based on the reference velocity (v_x) and initial robot height (H), the initial hip joint angles ($q(0)$), initial joint velocities ($\dot{q}(0)$), a threshold on the magnitude of gravity vector (r_{th}), and a threshold on track torques (τ_{th}) are set. The track actuator's torque (τ_{track}), roll (θ_R) and pitch (θ_P) from the IMU, and hip joint angles (q_{hip}) data are continuously read through encoders. Torque-based control manages the hip joints by considering the torque requirement on the same foot's track actuator (τ_i). When the tracked foot approaches an obstacle, an increase in torque requirement is experienced. Once the torque requirement exceeds the threshold (τ_{th}), torque-based control provides a pulsed input (Δq_τ) to open the hip joint, determined by the reference velocity (v_x) and a gain (G_τ). Similarly, when the torque requirement falls below the threshold (τ_{th}), the hip joint closes in the same proportion ($-G_\tau v_x$). IMU-based control manages the base orientation using θ_R and θ_P angles from the IMU sensor. This data computes a gravity vector $\vec{r}_g$, providing the magnitude $||\vec{r}_g(t)||$ and orientation ϕ_{rg} of the base, as shown in Fig. 7. Based on the quadrant in which ϕ_{rg} exists, the respective hip is actuated to compensate for changes in body orientation. Additionally, the diagonal hip joint is closed to maintain balance. Hip opening and closing are facilitated by pulsed input (Δq_{imu}), determined by the reference velocity (v_x) and a gain (G_{imu}). Different gains allow for weighted control of the hip joints. Furthermore, pulsed inputs from torque-based control (Δq_τ) and IMU-based control (Δq_{imu}) are accumulated and added to the respective hip positions (q_{hip}). To keep the robot base at a safe distance from the ground, a limit on the base height regulates hip joint angles, preventing them from opening beyond the upper limit

Algorithm 1 Proposed StabiliTrack Algorithm

Input: Torque on foot motors $\tau_{track} = [\tau_5, \tau_6, \tau_7, \tau_8]$, roll and pitch of the base θ_R, θ_P, forward velocity of base v_x
Output: Desired hip joint angle $q_{hip} = [q_1, q_2, q_3, q_4]$

procedure COMPUTE ROBOT CONFIGURATION BASED ON TRACKED FOOT TORQUE AND IMU DATA
  Set v_x, $q_i(0)$, $\dot{q}_i = 0, r_{th}$ ▷ Initial configuration
  $||\vec{r}_g(t)|| \leftarrow 0, \phi_{rg} \leftarrow 0$
  while StabiliTrack is on **do**
    Read current τ_{track}, θ_R, θ_P, q_{hip}
    Update Gravity Vector $\vec{r}_g$
    /* Torque-Based Control */
    if $\tau_{4+i} > \tau_{th}$ **then**
      $\Delta q_\tau[i] \leftarrow G_\tau v_x$ ▷ joint open
    else
      $\Delta q_\tau[i] \leftarrow -G_\tau v_x$ ▷ joint close
    /* IMU-Based Control */
    if $||\vec{r}_g|| > r_{th}$ **then**
      if $0 < \phi_{rg} < \pi/2$ **then**
        $i \leftarrow 5$
      else if $\pi/2 < \phi_{rg} < \pi$ **then**
        $i \leftarrow 6$
      else if $\pi < \phi_{rg} < 3\pi/2$ **then**
        $i \leftarrow 7$
      else
        $i \leftarrow 8$
      if $i < 7$ **then**
        $j \leftarrow i + 2$
      else
        $j \leftarrow i - 2$
      $\Delta q_{imu}[i] \leftarrow G_{imu} v_x$ ▷ joint open
      $\Delta q_{imu}[j] \leftarrow -G_{imu} v_x$ ▷ diagonal joint close
    $q_{hip} \leftarrow q_{hip} + \Delta q_\tau + \Delta q_{imu}$
    for $i = 1$ to 4 **do**
      if $q_{hip}[i] > q_{ulim}$ **then**
        $q_{hip}[i] \leftarrow q_{ulim}$
      else if $q_{hip}[i] < q_{llim}$ **then**
        $q_{hip}[i] \leftarrow q_{llim}$
  return q_{hip} ▷ Control action

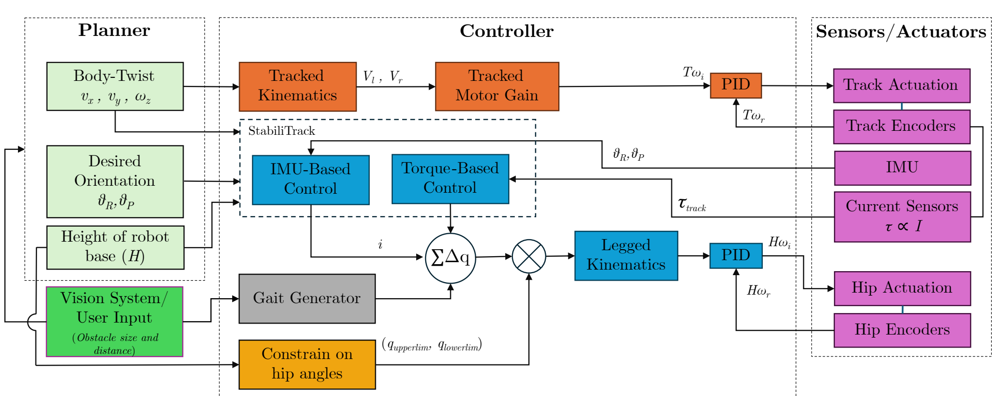

Fig. 6. Hierarchical control framework for TraQuad.

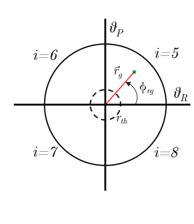

Fig. 7. Roll and pitch visualization for StabiliTrack algorithm.

Fig. 8. Tracked foot assembly with EM-Act modular actuator.

(q_{ulim}) or closing beyond the lower limit (q_{llim}). Hip positions (q_{hip}) are always corrected if any disturbance causes the hip to go beyond these limits.

III. Validation

To evaluate the performance of the tracked robot, multiple experiments were conducted in various scenarios. Initially, a single foot with an actuator was tested on a flat surface to understand its behavior. Subsequently, TraQuad's locomotion was assessed in both structured and natural environments. The results of these tests are discussed separately in the following subsections.

A. Experiments with single tracked foot

To test the single-tracked foot, an experimental setup was prepared since the foot cannot be stable on its own. In this subsection, the experimental setup, the tests conducted, and the results obtained with a single actuator are discussed.

1) Experimental setup: To test the single-tracked foot, the actuator was first assembled with the tracked foot and the electronics were connected. The foot-actuator assembly is shown in Fig. 8. To facilitate the operation of the tracks on a platform, a ground plane that can be inclined was prepared. Two T-section profile extrusions of 2 m were placed on a flat surface and fastened together with two additional T-section profiles to create a 2 m × 0.5 m rectangular frame. At the far ends of the frame, two poles of T-section profiles were placed in the center and their top ends were connected with another 2 m long profile.

A linear guide was mounted at the bottom side of the top 2 m long profile, allowing the foot to slide on the guide. A flat plywood was fixed on the rectangular frame and rubber mats were placed on its surface. The actuator with the tracked foot was then mounted on the linear guide as shown in Fig.9 and the frame height and the foot-actuator assembly were adjusted to ensure the foot gently grips the rubber mat. The height at the center and ends was matched to prevent changes in traction force due to variations in reaction force.

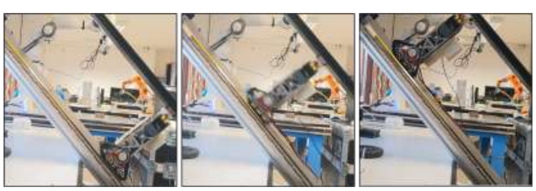

Fig. 9. Testing tracked foot with actuator EM-Act at a slope of 45°.

Fig. 10. The rotation of tracked actuator about hip joint (q_1), and the rotation of the tracked foot about the ankle joint (q_5). When the foot is lifted track orientation can be changed to approach an obstacle.

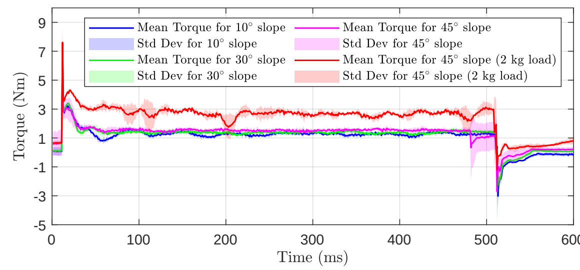

Fig. 11. Torque requirements to move a single tracked foot on various slopes and loading conditions.The peak torque is 4.67 Nm.

2) Experimental tests: With the foot-actuator setup, track limits were tested by varying the slope angle. Starting on a flat surface (0°), the angle was increased to 45°. The slope was limited to 45° as steeper inclines are not expected to be encountered. The system weighs about 1.1 kg with electronics, fasteners, and mountings. Additionally, the tracked foot's ability to pull the system with an extra 2 kg payload on a 45° slope was tested. The load is a metal disc attached to the actuator with a thread, allowing it to slide on the rubber mat. Tests were conducted at a forward velocity of v_x = 0.5 m/s, running the system for 2 s over 0.5 m.

Further, to test hip and ankle rotations simultaneously, the hip actuator was fixed on a flat surface of a table, and both the hip and ankle joints were actuated. The hip joint enables the leg to lift and avoid obstacles, while the pitch rotation of the ankle provides an approach angle aiding in foot placement on elevated, uneven surfaces with the required orientation. The foot's orientation changes due to friction within foot parts and the rolling resistance of the belt when lifted. Fig. 10 shows the hip and pitch rotations of the foot about its mounting axis.

3) Experimental results: Self-weight carrying tests were conducted on ground inclinations of 10°, 30°, and 45°. The robot successfully translated from start to endpoint in all tests. The mean and standard deviation of torque requirements during the experiments are shown in Fig. 11. Peak torque is required only during motion initiation and braking. The torques needed for 10°, 30°, and 45° slopes are similar, with a maximum peak mean-torque of 7.27 Nm for the 30° slope and a maximum mean-torque of 1.83 Nm during non-peak phases (30-550 ms). With an additional 2 kg load on the 45° slope, the peak mean-torque increases to 7.61 Nm, and the maximum mean-torque for non-peak phases is 3.5 Nm (30-550 ms). Acceleration during torque peaks is similar across all cases, reaching a maximum of 4.78 m/s^2. During non-peak phases, to maintain constant velocity, acceleration fluctuates around 0, with a maximum peak of 0.3 m/s^2 for non-loading cases and 1.25 m/s^2 for the 2 kg load case.

B. Experiments with TraQuad

To evaluate TraQuad's performance, five experiments were conducted: steering, slope climbing, obstacle climbing, obstacle skipping, and stepping on obstacles in both laboratory and natural settings.

1) Steering Test: In this test, TraQuad operates on a plane surface. Both straight rolling and skid steering are evaluated by executing a 'figure of 8' maneuver with a turning radius of 0.25 m. The tracing of the center of the base during this test is illustrated in Fig. 12. Additionally, the robot is capable

Fig. 12. TraQuad steering with tracked wheels (Turning radius = 0.25 m). The pink line showcases the tracking of the center of the robot's base link.

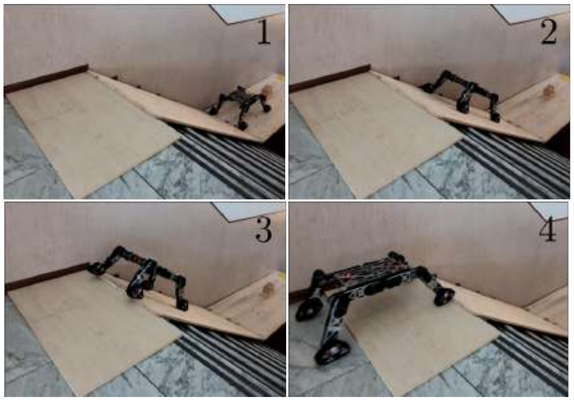

Fig. 13. TraQuad climbing a slope of 31° using tracked wheels at a velocity of 0.9 m/s. Phases: 1- front tracks butt the inclined slope, 2 robot climbing on the slope, 3- front tracks reached the top corner of the slope, - rear tracks reached the top corner of the slope.

to execute sharp turns by steering around its central vertical axis, utilizing opposite rotations on the left and right tracks.

2) Slope Climbing Test: In this test, TraQuad ascends a 3 m ramp with a 31° slope. The robot starts 1 m before the ramp and continues 1 m beyond it. The initial test velocity is 0.25 m/s, incrementally increased by 0.1 m/s until the robot fails to ascend. The maximum successful climbing velocity is 0.9 m/s, with the climbing sequence at $\vec{V} = 0.9$ m/s shown in Fig. 13. At $\vec{V} = 0.5$ m/s, the peak torque requirements for the tracks and hip joints are 1.70 Nm and 3.54 Nm, respectively. Peak acceleration occurs during initiation and braking at 0.1 m/s^2 and -0.1 m/s^2. At $\vec{V} = 0.9$ m/s, torque requirements for the tracks and hips are detailed in Fig. 14 and Fig. 15, with peak values of 4.38 Nm and 4.67 Nm. Peak acceleration reaches 0.16 m/s^2 and -0.19 m/s^2. A 3rd-order Savitzky-Golay filter with a 101-sample window is applied for torque data analysis. In phase 1, as the front tracks approach the slope, the torque requirement on the LH track increases, indicating it is trying to push the robot. This torque requirement balances out in phases 2 and 3. In phase 4, the RF track reaches the corner slightly earlier than the LF track, resulting in an earlier peak in torque requirement on the RF hip compared to the LF hip.

3) Obstacle Climbing Test: In this experiment, TraQuad climbs a 160 mm rock ($\approx$1.75 $\times$ track height) with a 50° slope. Using only tracked locomotion, the robot fails to ascend. Successful climbing requires base orientation manipulation,

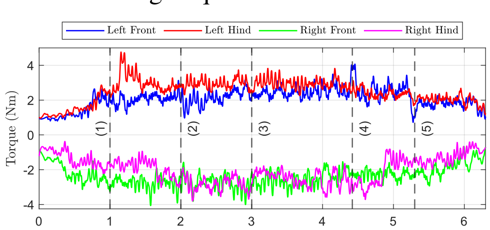

Fig. 14. Tracked foot torques of TraQuad climbing a slope of 31° with forward base velocity $v_x = 0.9$ m/s. The peak torque is 4.38 Nm.

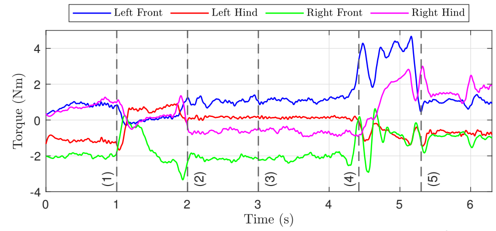

Fig. 15. Hip torques of TraQuad climbing a slope of 31° with forward base velocity $v_x = 0.9$ m/s. The peak torque is 4.67 Nm.

necessitating a legged-tracked control strategy. Alg.1 enables simultaneous hip actuation to lift the foot while progressing with tracks, facilitating ascent. The climbing sequence is depicted in Fig.16. In phase 1, only the tracks are engaged. As the left front (LF) track approaches the slope, the base tilts, prompting the LF hip to extend and restore horizontal orientation (phase 2). When the track descends, the hip retracts to reestablish balance (phase 3). This process repeats in phases 4-6. Notably, when tracing an obstacle's curvature, the climbing track requires higher velocity than the others. Thus, when a hip joint extends, its corresponding track maintains the command velocity, while the others rotate at a fraction of this speed. Torque requirements for the hip and track joints during this maneuver are shown in Fig.17 and Fig.18, respectively. The peak hip torque is 5.14 Nm (LF), while the maximum tracked foot torque is 1.88 Nm (LH).

4) Stepping on the Obstacle Test: In this test, TraQuad overcomes a 96 mm wooden block with a flat perpendicular edge in the front, which the robot finds difficult to overcome as the tracks cannot follow this profile and the foot overturns. To address this, the front foot is lifted and placed directly on the block, allowing the tracks to pull the robot forward. Since TraQuad lacks a vision system, the distance and size of the obstacle are manually provided to the gait generator, which calculates the hip opening angle required to step on the respective obstacle. Further, the rest of the forward motion is assisted by the StabiliTrack algorithm. Key phases of this maneuver are shown in Fig.19. In phase 1, to lift the left front (LF) foot, the right hind (RH) hip joint extends while the diagonal right front (RF) and left hind (LH) hip joints retract slightly, keeping the center of gravity within the support polygon. In phase 2, the LF foot lifts while the robot advances using the remaining tracks. In phase 3, the LF foot is placed on the block by adjusting the LF hip angle. In phase 4, StabiliTrack governs the forward motion. A similar procedure is applied to place the LH foot, requiring the RF foot to extend. Torque data for the hip and track joints during this task is shown in Fig.20 and Fig.21. The maximum continuous peak torque requirement for the hip joint (LF) is 8.15 Nm (LF, RF, RH), whereas, the maximum tracked foot torque requirement is 2.93 Nm (LF). Notably, in phases 1-2 and 5-6, the diagonal hip joints saturate (due to a torque limit placed in the controller), but this does not affect task execution.

5) Experiments in Natural Settings: In addition to laboratory experiments, tests were conducted in natural settings. To replicate real-world conditions, a test terrain was selected and modified with uneven ground and a combination of structured and unstructured obstacles, requiring the robot to climb, skip, or step over them. The terrain features six types of obstacles: gravel, stones/rocks, logs, wooden blocks, tree roots, and a pit

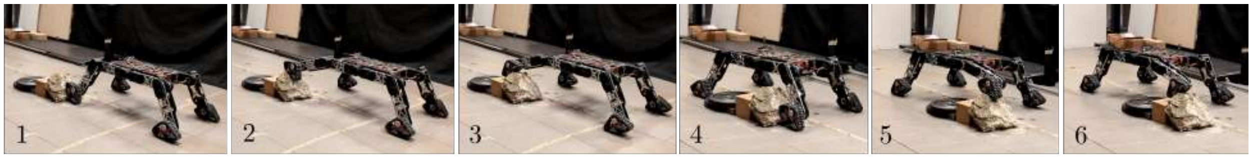

Fig. 16. TraQuad climbing a rock 1.75 times the height of its tracked foot and 50° slop using multi-modal locomotion. Phases: 1- LF track approaching the rock by opening the LF hip, 2- LF track is on the top of the rock while the hip is opened to accommodate the foot lift, 3- FL track is descending the rock by closing the hip. Similarly, 4- LH track approaching, 5- on top, and 6- descending the rock.

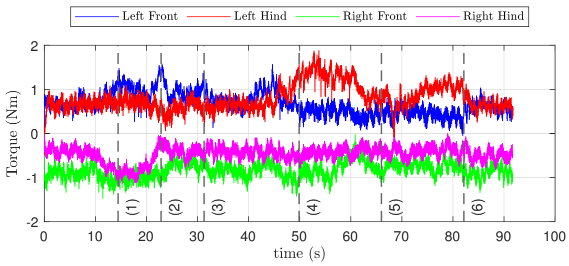

Fig. 17. Track joint torques of TraQuad climbing a rock 1.75 × tracked foot height using multi-modal locomotion. Max. joint torque is 1.88 Nm.

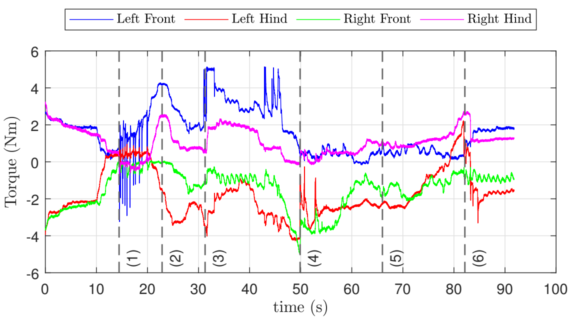

Fig. 18. Hip joint torques of TraQuad climbing a rock 1.75 × tracked foot height using multi-modal locomotion. Max. joint torque is 5.14 Nm.

with a step. Fig. 22 presents these obstacles along with their respective dimensions.

Different views of overcoming these obstacles are shown in Fig. 23. In phases 1-2, the hip joints adjust primarily due to torque-based control, as the torque requirements increase while climbing the stones. IMU-based control remains less dominant since the base orientation undergoes minimal change. In phases 3-4, a slight opening of the hip joints occurs in response to increased torque requirements on the foot while climbing the log. In phases 5-6, as the robot ascends a large rock, the torque requirement on the foot surpasses the threshold, accompanied by a significant change in base orientation, leading to the activation of both torque-based and IMU-based controls. In phases 7-8, a “Skip the Obstacle” maneuver is performed with a gait generator (refer Fig.6), where the foot does not step on the obstacle. To maintain the center of gravity within the support polygon of the other three feet, the gait generator positions the robot asymmetrically before lifting the foot. For this maneuver, obstacle distance and height are provided to the gait generator, which adjusts the foot-lifting motion accordingly. In phase 7, to lift the RF foot, the RF hip requires a peak torque of only 2.9 Nm. However, to support the asymmetric configuration and balance the robot, the LF hip requires 10.84 Nm and the RH hip requires 10 Nm peak torques. Similarly, in phase 8, to lift the RH foot, the RH hip provides a peak torque of 2.54 Nm. To support the asymmetric configuration, the LH hip requires 9.55 Nm and

TABLE II
ROBOT SPECIFICATIONS

No.	Property	Value
1	Maximum length	965 mm
2	Maximum width	288 mm
3	Maximum height	290 mm
4	Weight	6.9 kg
5	Rated joint torque	2.5 Nm
6	Peak joint torque	19.6 Nm
7	Battery capacity	4500 mAh
8	Control policy	PD control, StabiliTrack
9	Materials used	3-D printed ABS, aluminum
10	Slope climbing capability	31°

the RF hip requires 11.83 Nm peak torques. In phases 9-10, the robot encounters tree roots and stumps, where the control strategy mirrors that of phases 1-2. In phases 11-12, the robot descends a pit slope with a small step, rolls forward, ascends another step, and climbs the pit slope. Before the ascent, torque requirements and quadrant-based orientation changes remain minimal, leading to negligible hip angle adjustments. However, during the climb, an increase in torque requirements on the LF and LH feet causes the respective hips to open. At one point, the LF foot gets stuck, and upon release, the robot falls onto it, inducing a sudden shift in base orientation, which is counteracted by IMU-based control through the closing of the LF hip.

IV. DISCUSSION

In this paper, we explore the concept of combining two modalities of ground-based robot locomotion to traverse difficult terrains. We propose that merging tracked and legged robots can integrate the advantages of both systems into a single robot. Legged locomotion allows the robot to maneuver in highly uneven terrain, while tracks enable faster and more efficient navigation in relatively simpler terrains. Additionally, tracks as foot pads provide higher traction due to the larger contact patch area, and can deform to the shape of ground features, offering extra traction.

In the design validation, the track-actuator assembly tests demonstrate the capability to pull a 3.1 kg load (including self-weight) on a 45° slope at 0.5 m/s, requiring a peak torque of 7.27 Nm and a nominal torque of 3.5 Nm, which the actuator can provide easily. These findings confirm the potential of this actuator for track propulsion. Additionally, further tests on TraQuad to perform steering, slope climbing, obstacle climbing, stepping on, and skipping obstacles in lab and natural settings were successful. These results not only validate the use of EM-Act but also highlight effective strategies for navigating rough terrains with multi-modal locomotion.

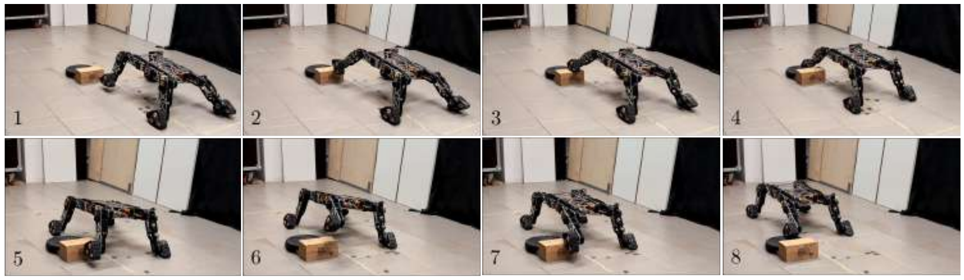

Fig. 19. TraQuad stepping on a block approximately equal to the height of its tracked foot using multi-modal locomotion. Phases: 1- RH hip extends bringing the robot in asymmetric configuration, 2-FL foot is lifted, 3- Robot moves forward and places FL foot on top of the block, 4- FL foot descends the block. Similarly, 5- RF hip extends, 6- LH foot is lifted, 7- Robot moves forward and places FL foot on top of the block, 8- LH foot descends the block.

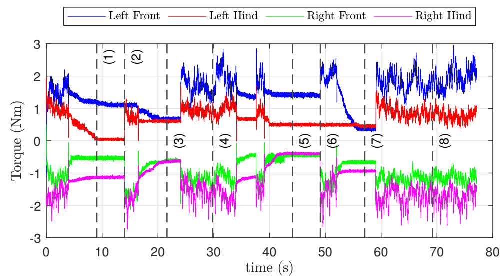

Fig. 20. Track joint torques of TraQuad stepping on a block equal to tracked foot height using multi-modal locomotion. Max. joint torque is 2.93 Nm.

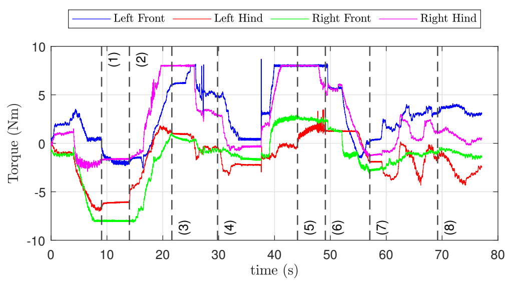

Fig. 21. Hip joint torques of TraQuad stepping on a block equal to the tracked foot height using multi-modal locomotion. Max. joint torque is 8.15 Nm.

TraQuad demonstrates an impressive slope-climbing capability, successfully ascending slopes of 31° at a velocity of 0.9 m/s, with peak torque requirements of 4.38 Nm on the tracks and 4.67 Nm on the hip joints. In comparison, the ANYmal-D robot can climb slopes up to 30°, albeit at a significantly slower pace. Multi-modal locomotion is employed in three scenarios: climbing, skipping, and stepping on obstacles. Obstacles such as rocks or scree with steep inclines are more effectively negotiated using tracks rather than stepping on walls or blocks. This advantage arises from the robot's ability to maintain contact with the rock surface, thereby leveraging the normal reaction force at the foot to reduce the load on the hip joints.

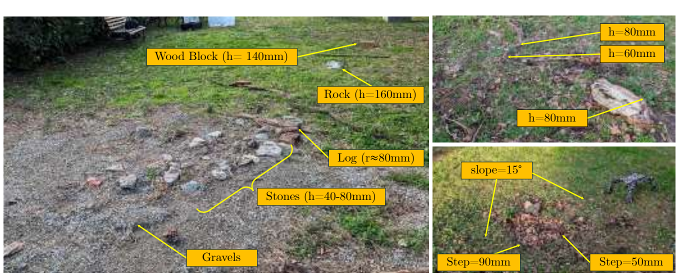

Fig. 22. Obstacles used in the tests performed in Natural Environments. Six types of obstacles are present: Gravels; Stones/Rock; Log; Wood Block; Tree roots; Pit with a step.

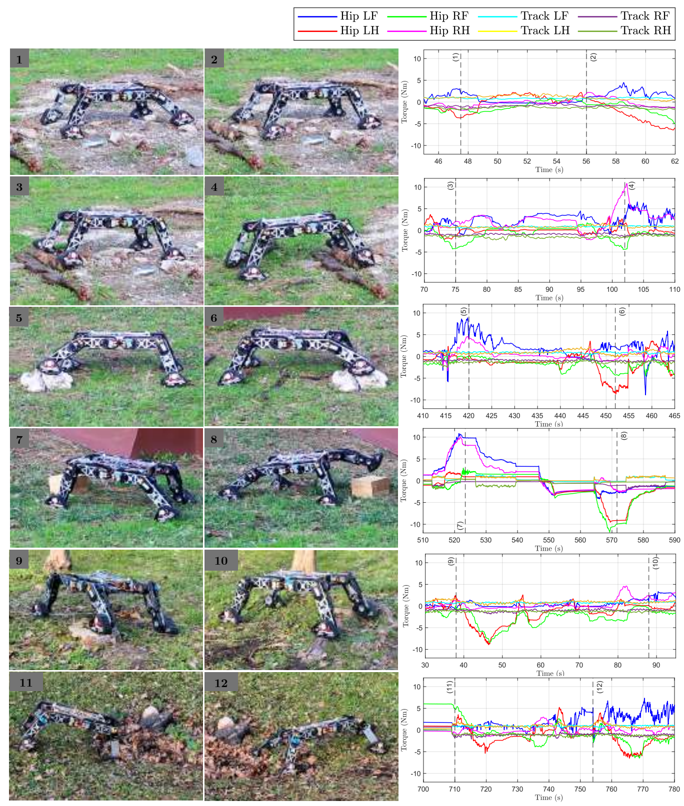

Fig. 23. Tests performed in Natural Environments. TraQuad in phases 1-2: traverses gravels and stones of 40-80 mm height, 3-4: climbs a log of 80 mm diameter, 5-6: climbs a rock of 160 mm height, 7-8: skips a wooden block of 140 mm height using gait-generator, 9-10: traverses a stump of 80 mm height and tree roots of 60-80 mm height, 11-12: descends and ascends a pit with 15° slope consisting 2 steps of 90 mm and 50 mm, respectively.

As illustrated in Fig. 18, during phases 1-3, when the left front (LF) foot ascends the rock, the LF knee torque peaks at 5.14 Nm, while the torques in the other three supporting hips remain comparatively lower. In contrast, Fig. 21 shows that when the LF leg steps on an obstacle, the torque in the diagonal hips (RF, LH) approaches the controller-imposed limit of 8.15 Nm. This increased torque demand arises from the asymmetry induced while repositioning the center of gravity (CG) within the support polygon. During phases 3-4, as the system is re-symmetrized, the torque burden shifts to the opposite diagonal hips (LF, RH). Once symmetry is restored, the torque requirements decrease substantially. A similar trend is observed in field tests on natural terrain, where obstacles were skipped using the RF and RH legs, as depicted in phases

TABLE III
SPECIFICATIONS OF POPULAR WHEELED-LEGGED ROBOTS. THE ASTERISK (*) REPRESENTS DATA UNAVAILABLE.

Robot	Height (m)	Max. Slope (°)	Obstacle Height (mm)	H./Obs. H.	Max. Speed (m/s)	DOFs	Weight (kg)
ANYmal-D	0.89	30	250	0.28	1.3	12	50
ANYmal Swiss-Mile	0.872	27	600	0.69	5	16	∼50
Ascento	0.66	*	400	0.60	2.22	6	10.4
Centauro	1.71	*	200	0.12	1.6	20 (legs)	92
TAWL	1.48	*	250	0.17	0.417	16	120
TraQuad	0.29	31	170	0.59	2	8	7

7-8 of Fig. 23. When the controller torque limit was removed, the maximum torque recorded while skipping a wood block 1.5 times the track height is 11.83 Nm.

In both experimental scenarios, the tracks consistently exhibited lower torque demands compared to the hip joints, with a peak torque of 2.93 Nm recorded during rock climbing. This observation underscores the efficiency of maintaining continuous ground contact. Consequently, a tracked-legged multi-modal variation is promising for uneven terrains for a faster, economical, and agile locomotion.

To demonstrate the effectiveness of TraQuad, its performance is compared with other notable hybrid robots mentioned in Sec.I. The properties of these robots are detailed in Tab. III. When comparing the ratio of the robot's height to its obstacle climbing capability (H./Obs. H.), TraQuad's ratio of 0.59 is commendable compared to other robots. A significant advantage of TraQuad is its ability to skip obstacles of this size/body ratio, whereas Swiss-mile and Ascento robots abilities are mentioned for step over or jump on obstacles of such ratio. Additionally, TraQuad is the lightest robot among the compared models, uses fewer actuators, and is faster than most of the other robots. Although the current configuration of TraQuad has limited off-road capabilities for performing different gaits, its performance is significant even in this minimal configuration (8-DOF version).

Though the current configuration of the robot has limited off-road capabilities for performing diverse legged gaits that a 12-DOF hybrid robot could offer, experimental validation shows that it performs well in both structured and natural environments. This reinforces our belief that this configuration is a significant first step towards tracked-legged multi-modal locomotion. By evaluating the 8-DOF robot, we aim to understand the potential achievements with a minimal configuration and the performance improvements that could be realized by increasing the DOF. This will help us determine that how many DOF are enough to encounter a certain level of obstacle and how many actuators are excessive and inefficient. This comparison will guide us in deploying the appropriate robot configuration for specific tasks.

V. CONCLUSION AND FUTURE WORK

Recent advancements in quadruped robot research have attracted significant attention due to their versatility and potential in navigating natural uneven terrains. To enhance the capabilities of quadrupedal robots, a modular tracked-legged robot, TraQuad, has been developed to perform multi-modal locomotion maneuvers effectively in rough terrains. To construct TraQuad, extensive testing of actuators for multi-modal locomotion was conducted, the robot was designed and prototyped, the control system was developed, and the StabiliTrack algorithm was implemented to navigate and overcome structured obstacles and rocks. Successful demonstrations have highlighted the potential of multi-modal robots as essential solutions for overcoming challenging obstacles that uni-modal designs struggle with. Future work will focus on enhancing this design by incorporating a knee joint with an additional actuator in the leg. A 12-DOF version of this robot, named TraQuad II, is currently under development, with its preliminary design presented in Fig. 24.

Fig. 24. The TraQuad II initial phase robot prototype (12-DOF).

REFERENCES

[1] F. Angelini *et al.*, "Robotic monitoring of habitats: The natural intelligence approach," *IEEE Access*, vol. 11, pp. 72 575–72 591, 2023.
[2] A. Ranjan *et al.*, "Design guidelines for bioinspired adaptive foot for stable interaction with the environment," *IEEE/ASME Transactions on Mechatronics*, vol. 29, no. 2, pp. 843–855, 2023.
[3] M. Hutter *et al.*, "Toward combining speed, efficiency, versatility, and robustness in an autonomous quadruped," *IEEE Transactions on Robotics*, vol. 30, no. 6, pp. 1427–1440, 2014.
[4] Y. Gao, *Contemporary planetary robotics: an approach toward autonomous systems*. John Wiley & Sons, 2016.
[5] R. Lindemann *et al.*, "Mars exploration rover mobility assembly design, test and performance," in *2005 IEEE International Conference on Systems, Man and Cybernetics*, vol. 1, 2005, pp. 450–455 Vol. 1.
[6] E. Lakdawalla, "The design and engineering of curiosity," *The Design and Engineering of Curiosity*, 2018.
[7] S. Li *et al.*, "Mobility performance evaluation of lunar rover and optimization of rocker-bogie suspension parameters," in *2008 2nd International symposium on systems and control in aerospace and astronautics*. IEEE, 2008, pp. 1–6.
[8] B. D. Harrington *et al.*, "The challenges of designing the rocker-bogie suspension for the mars exploration rover," in *37th Aerospace Mechanisms Symposium*, 2004.
[9] G. Reina *et al.*, "Wheel slippage and sinkage detection for planetary rovers," *IEEE/Asme Transactions on Mechatronics*, vol. 11, no. 2, pp. 185–195, 2006.
[10] B. Ghotbi *et al.*, "Mobility evaluation of wheeled robots on soft terrain: Effect of internal force distribution," *Mechanism and Machine Theory*, vol. 100, pp. 259–282, 2016.
[11] F. Zhou *et al.*, "Simulations of mars rover traverses," *Journal of Field Robotics*, vol. 31, no. 1, pp. 141–160, 2014.
[12] J. Y. Wong *et al.*, ""wheels vs. tracks"–a fundamental evaluation from the traction perspective," *Journal of terramechanics*, vol. 43, no. 1, pp. 27–42, 2006.
[13] L. Bruzzone *et al.*, "Locomotion systems for ground mobile robots in unstructured environments," *Mechanical sciences*, vol. 3, no. 2, pp. 49–62, 2012.
[14] P. Huang *et al.*, "Path tracking control of a differential-drive tracked robot based on look-ahead distance," *IFAC-PapersOnLine*, vol. 51, no. 17, pp. 112–117, 2018.
[15] Y. Fukuoka *et al.*, "Negotiating uneven terrain by a simple teleoperated tracked vehicle with internally movable center of gravity," *Applied Sciences*, vol. 12, no. 1, 2022.
[16] C. Zong *et al.*, "An angle-changeable tracked robot with human-robot interaction in unstructured environments," *Assembly Automation*, vol. 40, no. 4, pp. 565–575, 2020.
[17] Q.-H. Vu *et al.*, "Autonomous stair climbing algorithm for a small four-tracked robot," in *2008 International Conference on Control, Automation and Systems*. IEEE, 2008, pp. 2356–2360.

[18] B. M. Yamauchi, "Packbot: a versatile platform for military robotics," in *Unmanned ground vehicle technology VI*, vol. 5422. SPIE, 2004, pp. 228–237.

[19] D. Calisi *et al.*, "A semi-autonomous tracked robot system for rescue missions," in *2008 SICE Annual Conference*. IEEE, 2008, pp. 2066–2069.

[20] S. Habibian *et al.*, "Design and implementation of a maxi-sized mobile robot (karo) for rescue missions," *ROBOMECH Journal*, vol. 8, pp. 1–33, 12 2021.

[21] J. Ma *et al.*, "Design, simulation and manufacturing of a tracked robot for nuclear accidents," in *2014 IEEE International Conference on Robotics and Biomimetics (ROBIO 2014)*. IEEE, 2014, pp. 1828–1833.

[22] W. Chung *et al.*, "Wheeled robots," *Springer handbook of robotics*, pp. 575–594, 2016.

[23] D. Wettergreen, "Robotic walking on natural terrain: Gait planning and behavior-based control for statically-stable walking robots," Ph.D. dissertation, Carnegie Mellon University, Pittsburgh, PA, December 1995.

[24] G. Carbone *et al.*, "Legged robotic systems," in *Cutting Edge Robotics*, V. Kordic *et al.*, Eds. Rijeka: IntechOpen, 2005, ch. 33.

[25] "Anymal - a highly mobile and dynamic quadrupedal robot," in *2016 IEEE/RSJ International Conference on Intelligent Robots and Systems (IROS)*, 2016, pp. 38–44.

[26] B. Katz *et al.*, "Mini cheetah: A platform for pushing the limits of dynamic quadruped control," in *2019 International Conference on Robotics and Automation (ICRA)*, 2019, pp. 6295–6301.

[27] C. Semini *et al.*, "Design of the hydraulically actuated, torque-controlled quadruped robot hyq2max," *IEEE/Asme Transactions on Mechatronics*, vol. 22, no. 2, pp. 635–646, 2016.

[28] A. T. Spröwitz *et al.*, "Oncilla robot: a versatile open-source quadruped research robot with compliant pantograph legs," *Frontiers in Robotics and AI*, vol. 5, p. 67, 2018.

[29] A. Spröwitz *et al.*, "Towards dynamic trot gait locomotion: Design, control, and experiments with cheetah-cub, a compliant quadruped robot," *The International Journal of Robotics Research*, vol. 32, no. 8, pp. 932–950, 2013.

[30] L. Bruzzone *et al.*, "Functional design of a hybrid leg-wheel-track ground mobile robot," *Machines*, vol. 9, no. 1, p. 10, 2021.

[31] M. Bjelonic *et al.*, "A survey of wheeled-legged robots," in *Robotics in Natural Settings*, J. M. Cascalho *et al.*, Eds. Cham: Springer International Publishing, 2023, pp. 83–94.

[32] M. Schwarz *et al.*, "Hybrid driving-stepping locomotion with the wheeled-legged robot momaro," in *2016 IEEE International Conference on Robotics and Automation (ICRA)*, 2016, pp. 5589–5595.

[33] N. Kashiri *et al.*, "Centauro: A hybrid locomotion and high power resilient manipulation platform," *IEEE Robotics and Automation Letters*, vol. 4, no. 2, pp. 1595–1602, 2019.

[34] K. Xu *et al.*, "Adaptive impedance control with variable target stiffness for wheel-legged robot on complex unknown terrain," *Mechatronics*, vol. 69, p. 102388, 2020.

[35] J. He *et al.*, "Design and control of tawl—a wheel-legged rover with terrain-adaptive wheel speed allocation capability," *IEEE/ASME Transactions on Mechatronics*, vol. 27, no. 4, pp. 2212–2223, 2022.

[36] C. Grand *et al.*, "Decoupled control of posture and trajectory of the hybrid wheel-legged robot hylos," in *IEEE International Conference on Robotics and Automation, 2004. Proceedings. ICRA'04. 2004*, vol. 5. IEEE, 2004, pp. 5111–5116.

[37] M. Bjelonic *et al.*, "Whole-body mpc and online gait sequence generation for wheeled-legged robots," in *2021 IEEE/RSJ International Conference on Intelligent Robots and Systems (IROS)*, 2021, pp. 8388–8395.

[38] V. Klemm *et al.*, "Ascento: A two-wheeled jumping robot," in *2019 International Conference on Robotics and Automation (ICRA)*, 2019, pp. 7515–7521.

[39] L. Zhao *et al.*, "Compliant motion control of wheel-legged humanoid robot on rough terrains," *IEEE/ASME Transactions on Mechatronics*, pp. 1–11, 2023.

[40] J. Zhang *et al.*, "An adaptive approach to whole-body balance control of wheel-bipedal robot ollie," in *2022 IEEE/RSJ International Conference on Intelligent Robots and Systems (IROS)*, 2022, pp. 12 835–12 842.

[41] A. Stentz *et al.*, "Chimp, the cmu highly intelligent mobile platform," *Journal of Field Robotics*, vol. 32, no. 2, pp. 209–228, 2015.

[42] R. Hodoshima *et al.*, "Development of track-changeable quadruped walking robot titan x-design of leg driving mechanism and basic experiment-," in *2010 IEEE/RSJ International Conference on Intelligent Robots and Systems*, 2010, pp. 3340–3345.

[43] R. k. M. Gopanunni *et al.*, "Em-act: A modular series elastic actuator for dynamic robots," *IEEE Open Journal of the Industrial Electronics Society*, vol. 5, pp. 468–480, 2024.

[44] R. Sullivan *et al.*, "Cohesions, friction angles, and other physical properties of martian regolith from mars exploration rover wheel trenches and wheel scuffs," *Journal of Geophysical Research: Planets*, vol. 116, no. E2, 2011.

[45] J. L. Martínez *et al.*, "Approximating kinematics for tracked mobile robots," *The International Journal of Robotics Research*, vol. 24, no. 10, pp. 867–878, 2005.

Alok Ranjan received the B.Tech. degree in Mechanical Engineering from the Krishna Institute of Engineering and Technology, India in 2012, M.Tech. degree in Structures and Design from the Indian Institute of Space Science and Technology, India in 2016, and M.Sc. in Biomedical Engineering from the University of Groningen, the Netherlands in 2020. Alok currently is a Ph.D. student in Robotics at the University of Pisa. His main research interests are design and control of bio-inspired and compliant mechanisms.

Francesco Iotti received his B.S. degree in Mechatronics Engineering from the University of Modena and Reggio Emilia, Italy in 2020, M.S. degree in Automation and Robotics Engineering from the University of Pisa, Italy in 2023, where he currently is a Ph.D. student in Robotics. His main research interests are multi-modal robot design and automatic control.

Franco Angelini Franco received a B.S. degree in computer engineering in 2013 and an M.S. degree (cum laude) in automation and robotics engineering in 2016 from the University of Pisa, Pisa, Italy. The University of Pisa also granted him a Ph.D. degree (cum laude) in robotics in 2020. Franco is currently an Assistant Professor at the University of Pisa. His main research interests are control of soft robotic systems, impedance planning, and robotic environmental monitoring.

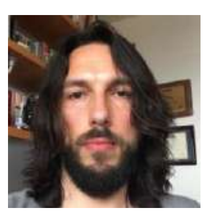

Manolo Garabini received his Ph.D. in Robotics from the University of Pisa, where he is now a Professor. His research focuses on designing, planning, and controlling soft adaptive robots. He is the Principal Investigator in the THING H2020 EU Research Project and has coordinated the Dysturbance H2020 Eurobench and H2020 EU Project Natural Intelligence.